



# Protein Kinase C- $\alpha$ Is a Gatekeeper of *Cryptosporidium* Sporozoite Adherence and Invasion

 Sayo McCowin,<sup>a</sup>  William A. Petri, Jr.,<sup>a,b,c</sup>  Chelsea Marie<sup>a</sup>

<sup>a</sup>Department of Medicine, Infectious Diseases and International Health, University of Virginia School of Medicine, Charlottesville, Virginia, USA

<sup>b</sup>Department of Pathology, University of Virginia School of Medicine, Charlottesville, Virginia, USA

<sup>c</sup>Department of Microbiology, Immunology and Cancer Biology, University of Virginia School of Medicine, Charlottesville, Virginia, USA

**ABSTRACT** *Cryptosporidium* infection is a leading cause of diarrhea-associated morbidity and mortality in young children globally. Single nucleotide polymorphisms (SNPs) in the human protein kinase C- $\alpha$  (*PRKCA*) gene region have been associated with susceptibility to cryptosporidiosis. Here, we examined the role of protein kinase C- $\alpha$  (PKC $\alpha$ ) activity in human HCT-8 intestinal epithelial cells during infection with *Cryptosporidium parvum* sporozoites. To delineate the role of PKC $\alpha$  in infection, we developed a fluorescence-based imaging assay to differentiate adherent from intracellular parasites. We tested pharmacological agonists and antagonists of PKC $\alpha$  and measured the effect on *C. parvum* sporozoite adherence to and invasion of HCT-8 cells. We demonstrate that both PKC $\alpha$  agonists and antagonists significantly alter parasite adherence and invasion *in vitro*. We found that HCT-8 cell PKC $\alpha$  is activated by *C. parvum* infection. Our findings suggest intestinal epithelial cell PKC $\alpha$  as a potential host-directed therapeutic target for cryptosporidiosis and implicate PKC $\alpha$  activity as a mediator of parasite adherence and invasion.

**KEYWORDS** *Cryptosporidium*, adherence, invasion, actin cytoskeleton, PKC $\alpha$ , susceptibility, *PRKCA*

*Cryptosporidium* spp. are a family of obligate intracellular parasites with increasing importance in global health. Although there are over 20 species relevant to humans, *Cryptosporidium parvum*, *C. hominis*, and *C. meleagridis* are responsible for the vast majority of infections (1–3). *Cryptosporidium* infection causes diarrhea that can be life-threatening, and in immunocompromised individuals (e.g., HIV/AIDS), this diarrhea can be prolonged. The burden of infection is most severe in low- and middle-income countries, with cryptosporidiosis being classified as the second leading cause of diarrhea-associated mortality in young children (4, 5). In addition to morbidity and mortality, pediatric cryptosporidiosis is associated with malnutrition and long-term developmental deficits (6–8). At present, no vaccine is available for cryptosporidiosis, and the only approved drug, nitazoxanide, has poor efficacy in immunocompromised patients and malnourished children (9, 10).

During human infection, *Cryptosporidium* oocysts excyst in the upper small intestine, presenting four sporozoites with gliding motility that interact with the mucosal epithelium (11, 12). These motile sporozoites attach to the host epithelium through interactions with host cell surface ligands (13) and sporozoite surface lectins (14, 15). Upon interaction, glycoproteins on the surface of the host cell membrane initiate a signaling cascade aggregating filamentous actin (F-actin) to the site of sporozoite contact and form a host membrane protrusion resulting in the encapsulation of the sporozoite (16–18). Henceforth, *Cryptosporidium* exists in an intracellular yet extracytoplasmic vacuole formed by and partitioned off from the host cell by F-actin (19). The formation of this F-actin pedestal at the site of infection has been directly linked to the actin-associated signaling pathways of the

**Editor** Andreas J. Bäuml, University of California, Davis

**Copyright** © 2022 McCowin et al. This is an open-access article distributed under the terms of the [Creative Commons Attribution 4.0 International license](#).

Address correspondence to Chelsea Marie, csm8r@virginia.edu.

The authors declare no conflict of interest.

This article is a direct contribution from William A. Petri, a member of the *Infection and Immunity* Editorial Board, who arranged for and secured reviews by Adam Sateriale, Francis Crick Institute, and Chris Huston, University of Vermont.

**Received** 24 December 2021

**Accepted** 3 January 2022

**Accepted manuscript posted online** 18 January 2022

**Published** 17 March 2022

neural Wiskott-Aldrich syndrome protein (N-WASP) and the Arp2/3 complex (20). The membrane protrusions encapsulating *Cryptosporidium* during invasion are additionally dependent on localized volume increases mediated by glucose and water influxes (21, 22). The recruitment of Na<sup>+</sup>/glucose cotransporter (SGLT1) and aquaporin 1 (AQP1) to the site of infection contributes to this actin-dependent cellular invasion. Analysis of the *C. parvum* transcriptome during development has identified the expression of stage-specific genes over the course of infection (23–25). Paired with microscopy imaging, a timeline for *Cryptosporidium* development and propagation *in vitro* has been well characterized. This entire life cycle has been modeled *in vitro* primarily using immortalized cell lines (26). However, the complete host cell repertoire that is usurped by *Cryptosporidium* spp. to achieve this has not yet been described.

Many studies have identified factors involved in *Cryptosporidium* infection on both sides of the parasite-host interface (18, 27, 28). Recently, we found that variation within the *PRKCA* gene was associated with increased susceptibility to cryptosporidiosis in children (29). Here, we asked the question, Is human protein kinase C- $\alpha$  (PKC $\alpha$ ) mechanistically involved in *Cryptosporidium* infection *in vitro*? In a recent study, a high-throughput phenotypic screen identified a selective protein kinase C- $\alpha/\beta$ 1 (PKC $\alpha/\beta$ 1) inhibitor, Gö6976, as having potent anticryptosporidial activity *in vitro* (30). Gö6976 reduced infection of HCT-8 cells with both *C. parvum* and *C. hominis* at nanomolar doses with an EC<sub>50</sub> (half-maximal effective concentration) for inhibition of *C. parvum* infection coinciding with the reported Gö6976 half-maximal inhibitory concentration (IC<sub>50</sub>) for PKC $\alpha$  (31). Furthermore, HCT-8 cell *PRKCA* mRNA expression has been shown to be significantly decreased after *C. parvum* infection compared to controls (32). From this evidence, we focused on exploring human intestinal epithelial cell PKC $\alpha$  further during *Cryptosporidium* infection.

In this study, we investigated the role of human intestinal epithelial cell PKC $\alpha$  during *C. parvum* infection *in vitro*. PKC $\alpha$  has been implicated in the regulation of host actin cytoskeletal remodeling, a requirement of parasite invasion; therefore, we targeted PKC $\alpha$  activity during this event. We found that PKC $\alpha$  mediated the earliest stages of *C. parvum* infection, sporozoite adherence and invasion, in human intestinal epithelial cells. Additionally, host PKC $\alpha$  was activated during sporozoite invasion. Our work exposes PKC $\alpha$  as a potential anticryptosporidial host target through inhibition of *C. parvum* adherence and invasion. Collectively, this work advances the understanding of *Cryptosporidium* pathogenesis and links a host protein to early infection.

## RESULTS

***C. parvum* activates host PKC $\alpha$  during invasion.** We investigated PKC $\alpha$  localization as a measure of activation during *C. parvum* invasion of HCT-8 cells. After binding the requisite cofactors for activation (phosphatidylserine, calcium, and diacylglycerol), activated PKC $\alpha$  translocates from the host cytoplasm to the membrane (33). We used a traditional *in vitro* fluorescence-based microscopy assay to simultaneously visualize *C. parvum* and intestinal epithelial cell PKC $\alpha$ . As a positive control for the activation of PKC $\alpha$ , we treated HCT-8 cells with phorbol-12-myristate 13-acetate (PMA). PMA is a well-established activator and induces the translocation of PKC to the cell membrane, where it is tightly bound and highly active (34–36). As predicted, exposure to 200 nM PMA for 1 h caused ubiquitous PKC $\alpha$  colocalization with the host membrane (Fig. 1A). Contrarily, we observed a decrease in membrane-associated PKC $\alpha$  when HCT-8 cells were treated with the PKC $\alpha$  inhibitor Gö6976 (2.5 nM) for 1 h (Fig. 1A). When HCT-8 cells were infected with *C. parvum* sporozoites at a multiplicity of infection (MOI) of 4:1 (sporozoite/cell ratio) for 2 h, we observed an increase in membrane-associated PKC $\alpha$  (Fig. 1A). Notably, the increase in *C. parvum*-induced membrane-associated PKC $\alpha$  is not limited to the *Cryptosporidium*-infected HCT-8 cell but can result in adjacent uninfected HCT-8 cell PKC $\alpha$  activation, suggesting a cell-to-cell signaling event during invasion.

To confirm *C. parvum* activation of intestinal epithelial cell PKC $\alpha$ , we examined this interaction using quantitative immunoblotting. We performed cellular fractionation of

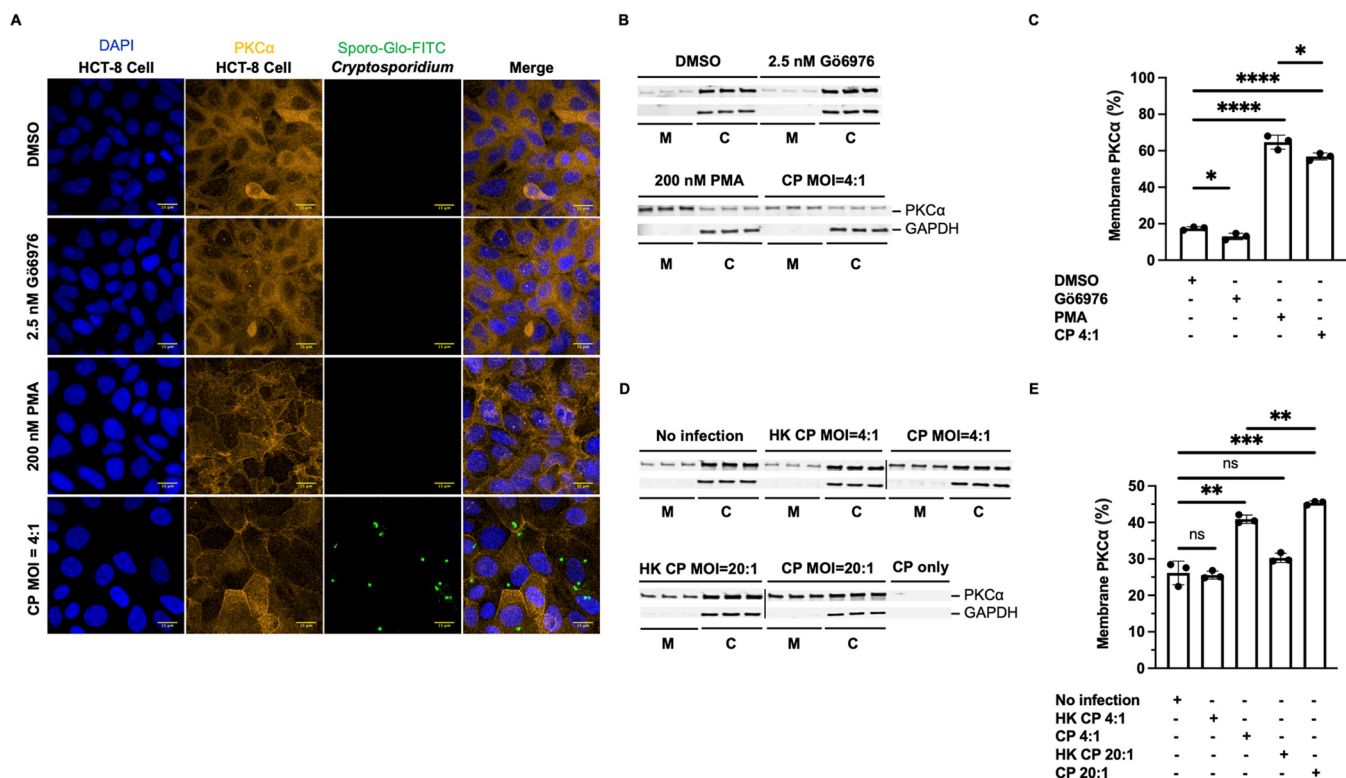


**FIG 1** *C. parvum* activates host PKC $\alpha$  during invasion. (A) Intestinal epithelial cells were treated with DMSO, 2.5 nM Gö6976, 200 nM PMA, or *C. parvum* (CP) at an MOI of 4:1 as described in Materials and Methods. High-magnification (63 $\times$  objective) confocal fluorescence microscopy images of DAPI (HCT-8 cell nucleus), anti-PKC $\alpha$ -Cy3 (PKC $\alpha$ ), FITC-conjugated Sporo-Glo (total *C. parvum*), and merged channels are shown. Data from one of two independent experiments are shown. (B) Intestinal epithelial cells were treated with DMSO, 2.5 nM Gö6976, 200 nM PMA, or *C. parvum* at an MOI of 4:1. Immunoblots of cell membrane (M) and cytoplasmic (C) fractions are displayed in biological triplicate ( $n = 2$ ). (C) Bar graph depicting quantification of membrane-associated PKC $\alpha$  (activation) after exposure to treatment. (D) Intestinal epithelial cells were treated with infection medium, heat-killed (HK) *C. parvum* at an MOI of 4:1, live *C. parvum* at an MOI of 4:1, HK *C. parvum* at an MOI of 20:1, or live *C. parvum* at an MOI of 20:1 for 2 h. Immunoblots of cell membrane and cytoplasmic fractions without *C. parvum* or with HK *C. parvum* at an MOI of 4:1, live *C. parvum* at an MOI of 4:1, HK *C. parvum* at an MOI of 20:1, and live *C. parvum* at an MOI of 20:1 are displayed in biological triplicate ( $n = 2$ ). (E) Bar graph depicting quantification of membrane-associated PKC $\alpha$  (activation) after exposure to treatment. Asterisks denote the results of one-tailed unpaired Student's *t* test used to analyze PKC $\alpha$  membrane association (\*,  $P < 0.05$ ; \*\*,  $P < 0.01$ ; \*\*\*,  $P < 0.001$ ; \*\*\*\*,  $P < 0.00001$ ; ns, not significant).

HCT-8 cells after treatment with 2.5 nM Gö6976, 200 nM PMA, or *C. parvum* at an MOI of 4:1. We generated cytoplasmic and membranous fractions and probed all fractions for glyceraldehyde 3-phosphate dehydrogenase (GAPDH) and PKC $\alpha$ . GAPDH localizes to the host cell cytoplasm, is constitutively expressed and stable in HCT-8 cells, and was used to denote the cytoplasmic fraction. We confirmed that pharmacological inhibition with Gö6976 decreased membrane-associated PKC $\alpha$ , while treatment with PMA resulted in increased membrane-associated PKC $\alpha$  (Fig. 1B). After infection with *C. parvum*, we observed increased membrane-associated PKC $\alpha$  (Fig. 1B). The percentage of PKC $\alpha$  in the membranous fraction after infection with *C. parvum* is significantly elevated ( $39.29\% \pm 1.235\%$  [ $P < 0.0001$ ]) relative to the vehicle controls (Fig. 1C). Next, we asked if the activation of PKC $\alpha$  during *C. parvum* invasion correlated with the rate of HCT-8 cell infection. To address this, we tested if heat-killed *C. parvum* sporozoites were capable of activating PKC $\alpha$  (Fig. 1D). Heat-killed *C. parvum* sporozoites did not induce a significant difference in membrane-associated PKC $\alpha$  relative to the vehicle controls (Fig. 1E). This phenotype remained true when increasing the MOI for heat-killed *C. parvum* to 20:1 (Fig. 1E). Furthermore, we increased the MOI of live *C. parvum* to 20:1, compared PKC $\alpha$  in the membranous fraction (Fig. 1D), and found that elevating the MOI resulted in a significant increase in membrane-associated PKC $\alpha$  ( $19.20\% \pm 1.902\%$  [ $P = 0.0005$ ]), supporting the activation of PKC $\alpha$  by *C. parvum* sporozoite invasion (Fig. 1E). Moreover, when comparing membrane-associated PKC $\alpha$  for live *C. parvum* at an MOI of 4:1 to that at an MOI of 20:1, we observed an additional significant

increase ( $4.522\% \pm 0.7185\%$  [ $P = 0.0033$ ]) (Fig. 1E). Altogether, these findings show that host intestinal epithelial cell PKC $\alpha$  is activated during *C. parvum* invasion *in vitro* in two distinct assays.

**A stoplight assay for differentiation of sporozoite adherence from invasion.** To distinguish the earliest steps of *C. parvum* infection, adherence and invasion, we developed a dual-color “stoplight” immunofluorescence assay (IFA). Antibody labeling of *C. parvum*-infected HCT-8 cells has been established previously to measure *C. parvum* development and propagation (37). However, we aimed to characterize sporozoite invasion, which is complete in 2 h *in vitro* after exposure to *C. parvum* sporozoites (18, 38, 39). To differentiate sporozoite adherence and invasion, we used two identical *C. parvum*-specific antibodies, conjugated to different fluorophores, coupled with staining before and after cell permeabilization (see Fig. S1A in the supplemental material). This assay was tested using *C. parvum*-infected HCT-8 cells to determine the assay selectivity for *C. parvum* sporozoite adherence and invasion. We report two distinct populations of labeled *C. parvum*-infected HCT-8 cells representative of sporozoite adherence and invasion (Fig. S1B). Adherent *C. parvum* sporozoites are dually labeled with fluorescein isothiocyanate (FITC)-conjugated Sporo-Glo (a monoclonal antibody that binds to *Cryptosporidium*) and tetramethylrhodamine isothiocyanate (TRITC)-conjugated Sporo-Glo, while invaded sporozoites are singly labeled with FITC-conjugated Sporo-Glo only. We performed single-antibody stains of *C. parvum*-infected HCT-8 cells separately and observed no spectral overlap between the FITC and TRITC fluorophores (Fig. S2A). Additionally, we stained *C. parvum*-infected HCT-8 cells with both antibodies simultaneously and observed 100% dually labeled sporozoites, as expected (Fig. S2A). To further evaluate the specificity of our assay to discriminate sporozoite adherence from invasion, we challenged fixed HCT-8 cells with *C. parvum* sporozoites, which should support only parasite adherence. When fixed HCT-8 cells were exposed to *C. parvum*, we observed 100% dually labeled *C. parvum* sporozoites, characteristic of exclusively adherent sporozoites (Fig. S2B). Together, these results validate that our stoplight assay can distinguish *C. parvum* adherence from invasion.

**Pharmacological inhibition of PKC $\alpha$  decreases *Cryptosporidium parvum* infection.**

We chose Gö6976 as the primary antagonist for our *in vitro* inhibitor studies due to its previously defined anticryptosporidial activity at PKC $\alpha$ -selective concentrations (29) and because it prevented PKC $\alpha$  activation in uninfected HCT-8 cells (Fig. 1A and B). HCT-8 cells were assessed for Gö6976-induced cytotoxicity using two methods, propidium iodide (PI) staining and HCT-8 cell nucleus counts relative to dimethyl sulfoxide (DMSO)-treated controls (Fig. S3). Using the stoplight assay, we examined the effect of Gö6976 treatment of HCT-8 cells on *C. parvum* adherence and invasion. HCT-8 cells were treated with 2.5 nM Gö6976 for 1 h prior to infection with *C. parvum* sporozoites at an MOI of 4:1. At 2 h postinfection, we observed a significant reduction in adherent (FITC-positive [FITC<sup>+</sup>]/TRITC<sup>+</sup>) sporozoites for Gö6976-treated cells relative to the DMSO-treated controls (Fig. 2A). Treatment with Gö6976 reduced the total parasite number by 54.7% (26.5% to 12.0% [ $P < 0.0001$ ]) relative to the DMSO-treated controls, showing that Gö6976 has anticryptosporidial activity early in infection (Fig. 2C). The decrease in the total parasite number corresponded to decreases in sporozoite adherence by 67.5% (11.5% to 4.40% [ $P = 0.0038$ ]) and invasion by 45.1% (15.0% to 8.24% [ $P = 0.003$ ]) (Fig. 2C). At higher concentrations of Gö6976, 7.5 nM and 12.5 nM, we observed reductions in *C. parvum* total parasite numbers by 71.4% (19.7% to 5.65% [ $P = 0.001$ ]) and 84.4% (19.7% to 3.08% [ $P = 0.0002$ ]), respectively (Fig. 2D). This decrease in total parasite numbers corresponded to decreases in sporozoite adherence by 71.5% (10.8% to 3.07% [ $P = 0.0038$ ]) and 82.6% (10.8% to 1.87% [ $P = 0.0009$ ]) and invasion by 71.3% (8.99% to 2.58% [ $P = 0.0008$ ]) and 86.5% (8.99% to 1.21% [ $P < 0.0001$ ]), respectively (Fig. 2D). We calculated the EC<sub>50</sub> for Gö6976 inhibition of *C. parvum* invasion to be 1.99 nM (Fig. 2E), within a close range of the reported IC<sub>50</sub> of Gö6976 for PKC $\alpha$  (IC<sub>50</sub> = 2.3 nM) (31). We also evaluated the impact of Gö6976 treatment of *C. parvum* sporozoites independently and found no significant difference in the total parasite number or adherence to or invasion of HCT-8 cells relative to the

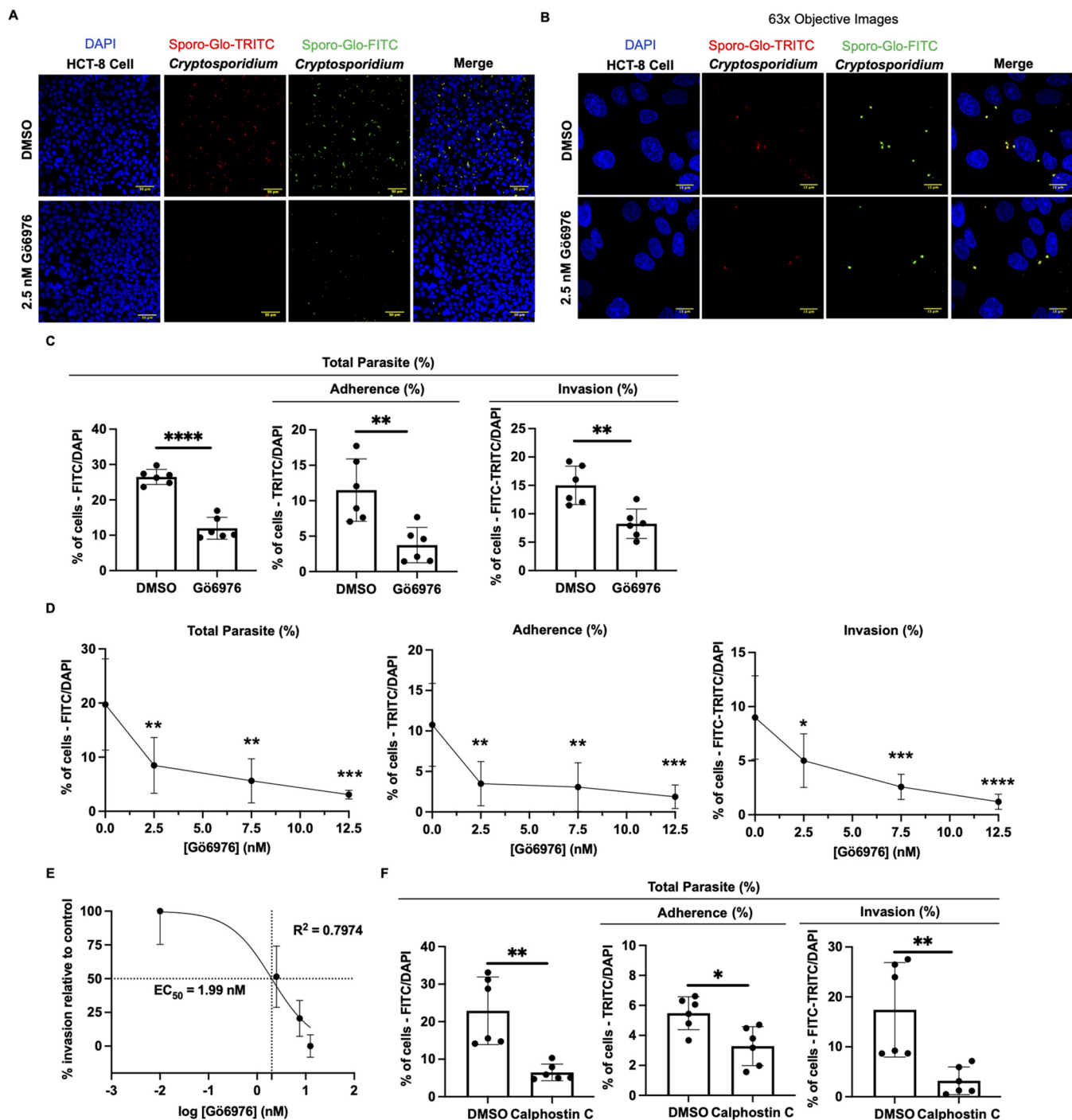


**FIG 2** Inhibition of PKC $\alpha$  decreases *Cryptosporidium parvum* adherence and invasion. (A) Confocal microscopy (20 $\times$  objective) images of DAPI (HCT-8 cell nucleus), TRITC-conjugated Sporoglo (adherent *C. parvum*), FITC-conjugated Sporoglo (total *C. parvum*), and merged channels. HCT-8 cells were treated with either DMSO (vehicle control) or 2.5 nM Gö6976 for 1 h. (B) High-magnification images (63 $\times$  objective) denoting differences in *C. parvum* total parasite number, adherence, and invasion. (C) Bar graph quantification from confocal microscopy images of *C. parvum* total parasite number and adherence to and invasion of HCT-8 cells after treatment with DMSO or 2.5 nM Gö6976. Data from one of two independent experiments are shown. (D) Concentration curve of treatment with increasing doses of Gö6976 and effect on *C. parvum* total parasite number, adherence, and invasion relative to the DMSO-treated control. Data from one of two independent experiments are shown. (E)  $EC_{50}$  calculation of Gö6976 treatment and *C. parvum* invasion. Gö6976 concentrations are log transformed, and percent invasion is relative to the DMSO-treated control. (F) Bar graph quantification of *C. parvum* total parasite number and adherence to and invasion of HCT-8 cells after treatment with DMSO or 50 nM calphostin C for 1 h. Data from one of two independent experiments are shown. For panels C and F, asterisks denote the results of one-tailed unpaired Student's *t* test (\*,  $P < 0.05$ ; \*\*,  $P < 0.01$ ; \*\*\*,  $P < 0.001$ ; \*\*\*\*,  $P < 0.00001$ ). For panel D, asterisks denote the results of one-way ANOVA and Tukey's *post hoc* test (\*,  $P < 0.05$ ; \*\*,  $P < 0.01$ ; \*\*\*,  $P < 0.001$ ; \*\*\*\*,  $P < 0.00001$ ).

**TABLE 1** Effect of PKC $\alpha$  pharmacological compounds on *C. parvum* total parasite number and adherence to and invasion of HCT-8 cells<sup>a</sup>

Compound	% change (mean % value for control $\pm$ SD–mean % value with treatment $\pm$ SD [ <i>P</i> value])		
	Effect on total parasite no.	Effect on adherence	Effect on invasion
Gö6976	↓54.7 (26.5 $\pm$ 2.13–12.0 $\pm$ 3.09 [ $<$ 0.0001])	↓67.5 (11.5 $\pm$ 4.40–3.74 $\pm$ 2.49 [0.0038])	↓45.1 (15.0 $\pm$ 3.38–8.24 $\pm$ 2.6 [0.003])
Calphostin C	↓71.7 (22.9 $\pm$ 9.00–6.47 $\pm$ 2.22 [0.0015])	↓40.1 (5.48 $\pm$ 1.10–3.28 $\pm$ 1.30 [0.01])	↓81.7 (17.4 $\pm$ 9.46–3.19 $\pm$ 2.76 [0.0054])
PMA	↑149 (26.5 $\pm$ 2.13–65.9 $\pm$ 5.14 [ $<$ 0.0001])	↑142 (11.5 $\pm$ 4.40–27.8 $\pm$ 5.46 [0.0002])	↑154 (15.0 $\pm$ 3.38–38.1 $\pm$ 8.52 [0.0001])
Bryostatin 1	↑126 (22.9 $\pm$ 9.00–51.8 $\pm$ 4.63 [ $<$ 0.0001])	↑225 (5.48 $\pm$ 1.10–17.8 $\pm$ 4.81 [0.0001])	↑95.4 (17.4 $\pm$ 9.46–34.0 $\pm$ 4.17 [0.0029])

<sup>a</sup>For all experiments, unpaired Student's *t* test was conducted to calculate statistical differences between means of groups of data.

DMSO-treated sporozoites (Fig. S4). This suggests that Gö6976 acts primarily via host PKC $\alpha$  inhibition as opposed to other kinases (e.g., PKC $\beta$ 1 or TrkA) that are targeted by Gö6976 at higher concentrations or a parasite effector.

To further test the importance of PKC $\alpha$ , we used an alternative inhibitor of PKC, calphostin C. Calphostin C induces the inhibition of PKC $\alpha$  through an independent mechanism from Gö6976, and importantly, this inhibition is irreversible, permitting the removal of the compound prior to *C. parvum* exposure. Calphostin C (50 nM) treatment of HCT-8 cells resulted in a reduction in the *C. parvum* total parasite number by 71.7% (22.9% to 6.47% [*P* = 0.0015]) relative to the DMSO-treated controls. This total parasite number decrease corresponded to decreases in sporozoite adherence by 40.1% (5.48% to 3.28% [*P* = 0.01]) and invasion by 81.7% (17.4% to 3.19% [*P* = 0.0054]) (Fig. 2F). These data are summarized in Table 1. Altogether, these data support a primary role for host PKC $\alpha$  in mediating both sporozoite adherence and invasion.

#### Pharmacological activation of PKC $\alpha$ increases *Cryptosporidium parvum* infection.

We next investigated the impact of the activation of PKC $\alpha$  on *C. parvum* adherence and invasion. Prior to infection, we activated PKC $\alpha$  by treating HCT-8 cells with PMA (200 nM) for 1 h. HCT-8 cells were assessed for PMA-induced cytotoxicity using PI staining and HCT-8 cell nucleus counts relative to DMSO-treated controls as described above (Fig. S3). Using the stoplight assay, at 2 h postinfection, we observed significant increases in both adherent and invaded (TRITC- and FITC-labeled) *C. parvum*-infected HCT-8 cells (Fig. 3A and B). PMA-treated HCT-8 cells showed an increase in the *C. parvum* total parasite number by 149% (26.5% to 65.9% [*P* < 0.0001]) (Fig. 3C). This increased total parasite number corresponded to increases in both sporozoite adherence by 142% (11.5% to 27.8% [*P* = 0.0002]) and invasion by 154% (15.0% to 38.1% [*P* = 0.0001]) relative to the DMSO-treated controls (Fig. 3C). The duration of exposure to PMA has been correlated with the degree of PKC $\alpha$  activation, with extended incubation leading to a paradoxical inhibition caused by ubiquitination and degradation (40, 41). To determine the optimal time required to achieve maximum PKC $\alpha$  activation in HCT-8 cells, we varied the length of exposure to PMA. We observed a rapid translocation of PKC $\alpha$  to the plasma membrane as early as 15 min after treatment with PMA (Fig. 3D). Since PMA-induced activation of PKC $\alpha$  occurred so rapidly, we next examined if priming of PKC $\alpha$  activation accelerates early *C. parvum* infection. To test this, we challenged HCT-8 cells with *C. parvum* and quantified the total parasite number at 15 min, 30 min, and 1 h with or without exposure to 200 nM PMA for 1 h. At the earliest recorded time point of 15 min, we observed an increase in the *C. parvum* total parasite number by 160% (12.8% to 33.3% [*P* < 0.0001]) (Fig. 3E). This increase in the *C. parvum* total parasite number was significant across all experimental time points relative to the DMSO-treated controls, resulting in increases of 131% (21.2% to 49.0% [*P* < 0.0001]) and 115% (25.9% to 55.6% [*P* < 0.0001]) at 30 min and 1 h, respectively (Fig. 3E). To determine if this increased *C. parvum* total parasite number was specific to PMA, we introduced an alternative pharmacological agonist of PKC $\alpha$ , bryostatin 1 (42). Bryostatin 1 activates PKC via binding to the C1 domain of PKC, which is distinct from PMA (43). At 2 h postinfection, bryostatin 1 treatment of HCT-8 cells for 20 min resulted in an increase in the *C. parvum* total parasite number by 126% (22.9% to 51.8% [*P* < 0.0001]) relative to the DMSO-treated controls (Fig. 3F). This increase in the total

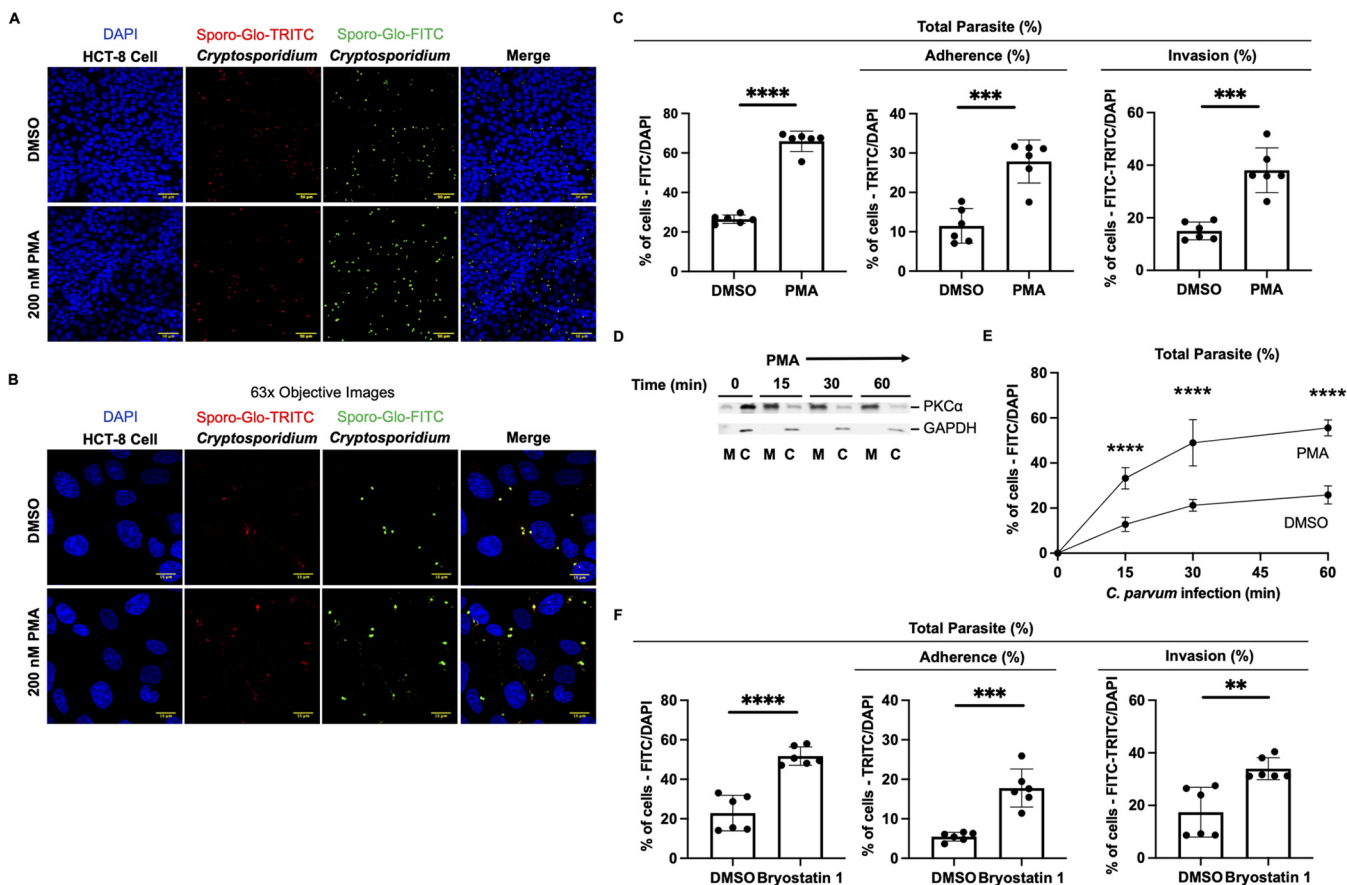


**FIG 3** Activation of PKC $\alpha$  increases *Cryptosporidium parvum* adherence and invasion. (A) Confocal microscopy (20 $\times$  objective) images of DAPI (HCT-8 cell nucleus), TRITC-conjugated Sporozo-Glo (adherent *C. parvum*), FITC-conjugated Sporozo-Glo (total *C. parvum*), and merged channels. HCT-8 cells were treated with either DMSO or 200 nM PMA for 1 h. (B) High-magnification images (63 $\times$  objective) denoting differences in *C. parvum* total parasite number and adherence to and invasion of HCT-8 cells. (C) Bar graph quantification from confocal microscopy images of *C. parvum* total parasite number and adherence to and invasion of HCT-8 cells after treatment with DMSO or 200 nM PMA. Data from one of two independent experiments are shown. (D) Immunoblots of membrane and cytoplasmic HCT-8 cell fractions treated with 200 nM PMA over time ( $n = 2$ ). (E) Time course of *C. parvum* infection with or without treatment with 200 nM PMA for 1 h relative to the DMSO-treated control. Data from one of two independent experiments are shown. (F) Bar graph quantification of *C. parvum* total parasite number and adherence to and invasion of HCT-8 cells after treatment with 100 nM bryostatin 1 or DMSO for 20 min. Data from one of two independent experiments are shown. For panels C and F, asterisks denote the results of one-tailed unpaired Student's *t* test (\*,  $P < 0.05$ ; \*\*,  $P < 0.01$ ; \*\*\*,  $P < 0.001$ ; \*\*\*\*,  $P < 0.00001$ ). For panel E, asterisks denote the results of one-way ANOVA and Tukey's *post hoc* test (\*,  $P < 0.05$ ; \*\*,  $P < 0.01$ ; \*\*\*,  $P < 0.001$ ; \*\*\*\*,  $P < 0.00001$ ).

parasite number corresponded to increases in sporozoite adherence by 225% (5.48% to 17.8% [ $P = 0.0001$ ]) and invasion by 95.4% (17.4% to 34.0% [ $P = 0.0029$ ]). These findings indicate that PKC $\alpha$  activation enhances *C. parvum* adherence and invasion.

## DISCUSSION

Two major findings emerged from this study. First, *C. parvum* activated PKC $\alpha$  in human intestinal epithelial cells. Second, host PKC $\alpha$  mediated the initial adherence of parasites as well as internalization resulting in invasion, which we discovered using our stoplight imaging assay. PKC $\alpha$  activity was directly related to parasite infection as pharmacological antagonists blocked *C. parvum* adherence and invasion, while pharmacological agonists promoted *C. parvum* adherence and invasion (Table 1). Our studies therefore provide insight into how polymorphisms in human *PRKCA* may increase susceptibility to cryptosporidiosis in children (29), suggesting that increased PKC $\alpha$  activity may increase permissibility to infection at the intestinal epithelium. We now have shown a novel role for host PKC $\alpha$  in *Cryptosporidium* adherence to and invasion of human intestinal epithelial cells. The facts that *Cryptosporidium* targets intestinal epithelial cell PKC $\alpha$  during early infection and PKC $\alpha$  activity is critical for a pathogenic host-mediated cellular process make it an attractive target for host-directed therapy.

Pharmacological inhibition of intestinal epithelial cell PKC $\alpha$  reduced, while activation of PKC $\alpha$  enhanced, *C. parvum* adherence and invasion. These findings implicate host PKC $\alpha$  activity in promoting both parasite adherence and invasion. Importantly, we observed that treatment with the competitive inhibitor Gö6976 and the irreversible antagonist calphostin C resulted in comparable reductions in adherence and invasion. Mechanistically, these compounds alter PKC $\alpha$  through dissimilar actions. Gö6976 inhibits PKC $\alpha$  through competition with ATP (31), while calphostin C inhibits PKC $\alpha$  through C1 domain binding (44, 45). The use of pharmacological antagonists to target PKC $\alpha$  with differing mechanisms of action further supports a role for PKC $\alpha$ -mediated parasite entry. Moreover, *C. parvum* sporozoites showed no significant difference in infection of intestinal epithelial cells upon treatment with Gö6976. This finding was expected as no known homologs of PKC $\alpha$  have been reported in any *Cryptosporidium* spp., adding additional support for a host-inhibitory effect. We additionally found that treatment with a PKC $\alpha$  agonist alters the kinetics of infection *in vitro*. Altogether, these findings confirm a role for PKC $\alpha$  in parasite adherence and invasion and suggest the activation of PKC $\alpha$  as a preliminary event to *C. parvum* infection.

PKC $\alpha$  alters the morphology of the host cell F-actin cytoskeleton, thereby regulating processes that are affected by the reorganization of these microfilaments (46, 47). PKC $\alpha$  is active at the cell membrane, the same site as parasite adherence and invasion. Hence, it is biologically plausible for PKC $\alpha$  to have activity at the host-parasite interface. Two kinases important for regulating actin polymerization have been implicated in the required rearrangement of F-actin during *Cryptosporidium* infection: proto-oncogene tyrosine-protein kinase Src (c-Src) and phosphatidylinositol 3-kinase (PI3K) (20, 48–50). Inhibition of c-Src via a dominant negative mutant blocked *C. parvum*-mediated rearrangement of F-actin and, subsequently, *C. parvum* invasion of human biliary epithelial cells (48). Similarly, genetic and pharmacological inhibition of PI3K decreased *C. parvum*-induced actin rearrangements and blocked invasion of human biliary epithelial cells (50). PKC $\alpha$  has been reported upstream to regulate c-Src (51, 52) and PI3K (53, 54). Although these studies did not discern parasite adherence from invasion, we speculate that sporozoite adherence results in the activation and recruitment of host PKC $\alpha$  to the cell membrane. This results in a PKC $\alpha$  phosphorylation cascade leading to the F-actin remodeling required for invasion (see Fig. S5 in the supplemental material). This research furthers our current understanding of the anticryptosporidial activity of PKC $\alpha$  antagonists by pinpointing activity to specific life cycle stages. Furthermore, we have established *C. parvum*-induced activation of PKC $\alpha$  as a critical event during invasion. Thus, PKC $\alpha$  is a key host protein target meriting further investigation as its activity will yield additional insight into the molecular mechanisms of parasite invasion.

Host-directed therapy is an emerging approach in the field of anti-infectives. Recent insights into pathogen-host interactions are leading to the identification of a wide array of host targets involved in pathogenesis. We show here that PKC $\alpha$  activity mediates *Cryptosporidium* adherence to and invasion of intestinal epithelial cells *in vitro*. Evidence from our *in vitro* analyses suggests that PKC $\alpha$  is a potential host target for therapy in human infection with *Cryptosporidium*, although further experimentation is necessary, in particular as our analysis examined only the addition of inhibitors prior to infection with sporozoites. Remarkably, there remains no PKC $\alpha$ -specific FDA-approved drug despite isozyme-specific contrasts in activity being linked to a number of human disease states (55–58). However, the PKC agonist bryostatin 1 is currently in phase 2 clinical trials for the treatment of moderately severe to severe Alzheimer's disease (59). Consequently, the pharmacological antagonists used in this study may serve as suitable options for future anticryptosporidial studies.

Using our fluorescence-based approach to examine PKC $\alpha$  activity, we observed the activation of PKC $\alpha$  in not only *Cryptosporidium*-infected cells but also adjacent uninfected intestinal epithelial cells. Our pharmacological data suggest that the host cell baseline PKC $\alpha$  activation state may determine hospitality to *Cryptosporidium* infection. Therefore, the activation of PKC $\alpha$  in adjacent uninfected intestinal epithelial cells may

have biological relevance. We speculate that PKC $\alpha$  activation in adjacent uninfected cells is the result of a cell contact signaling event. A host pathway for PKC activation has been found for other protozoan parasites during invasion (60). *Entamoeba histolytica* and *Cryptosporidium* spp. recognize the same surface sugar for adherence to human cells. We hypothesize that *Cryptosporidium* sporozoite adherence to an intestinal epithelial cell induces a rapid influx of calcium ions (Ca<sup>2+</sup>) and subsequently in adjacent uninfected cells through cellular gap junctions. The intracellular Ca<sup>2+</sup> influx activates host PKC $\alpha$  in *Cryptosporidium*-infected cells and adjacent uninfected cells. Delineating intracellular Ca<sup>2+</sup> signaling and PKC $\alpha$  activation during epithelial cell *Cryptosporidium* infection is an important next step.

This study directly builds on the identification of *PRKCA* in a forward genetic screen by defining a role experimentally, at an enzymatic level, for susceptibility in human intestinal epithelial cells *in vitro*. Our pharmacological analyses suggest that the previously identified polymorphisms in *PRKCA* would increase PKC $\alpha$  activity, via increased mRNA expression or protein stability. Furthermore, these data suggest that the polymorphisms associated with increased susceptibility act through exerting changes in the intestinal epithelium. Expression quantitative trait locus (eQTL) analyses have linked the associated SNPs with decreased *PRKCA* mRNA expression in the esophagus and colon (61). However, the impact on small intestinal expression, which is the major site of *Cryptosporidium* infection, has not been determined. Our findings suggest that SNPs associated with increased susceptibility to *Cryptosporidium* might act via increased PKC $\alpha$  activity during *Cryptosporidium* infection, either by increasing *PRKCA* mRNA expression or via compensatory gene regulation of PKC $\alpha$  regulators. Alternatively, the activation of human intestinal cell PKC $\alpha$  may be *Cryptosporidium* specific, resulting in altered expression only upon exposure to parasites.

A limitation of the *in vitro* system is that HCT-8 cells are cancer cells and may have aberrant PKC $\alpha$  activity (62). This concern is somewhat mitigated by the observation that PKC $\alpha$  was activated and inhibited as expected in HCT-8 cells. An additional limitation of our system is the inability to investigate the immune response to infection. Th17 cells have been implicated in the response to infection, with increased levels of Th17-related cytokines being reported in the gut (63), and PKC $\alpha$  is a positive regulator of Th17 cell function (64). Moreover, gut infection has been linked to immune-mediated alterations leading to functional changes in the intestinal epithelium (65). Here, modifications of intestinal epithelial cell actin-binding proteins, ezrin and villin, played a role in *Giardia* pathophysiology and are CD4<sup>+</sup> and CD8<sup>+</sup> T cell dependent (65). To address a secondary role for PKC $\alpha$  in the immune response to *Cryptosporidium* infection, further examination *in vivo* is needed. A major strength of this study is the identification of intestinal epithelial cell PKC $\alpha$  activation by *C. parvum*, which implicates yet another host kinase in infection. Second, we used a well-characterized intestinal cell model that allowed the examination of PKC $\alpha$  activity at precise stages of parasite infection. The use of this intestinal cell system also allowed the investigation of PKC $\alpha$  devoid of the influence of immune cell regulation. Finally, the introduction of the stop-light assay for the differentiation of parasite adherence from invasion and downstream quantification is an asset for future studies in the field.

In conclusion, using an *in vitro* system of intestinal epithelial cell cryptosporidiosis, we expand on the role of PKC $\alpha$  and susceptibility to infection. We elucidated the parasite stages in which PKC $\alpha$  is involved by demonstrating that changes in PKC $\alpha$  activity impact downstream *C. parvum* adherence and invasion. We show in this study that *C. parvum* sporozoites activate intestinal epithelial cell PKC $\alpha$  and prove that PKC $\alpha$  activation is critical for *C. parvum* adherence and invasion. These results lead us to conclude that the activation of PKC $\alpha$  by *C. parvum* is deliberate and an important component of infection of intestinal epithelial cells. Thus, the mechanisms by which PKC $\alpha$  promotes *C. parvum* invasion and its role *in vivo* warrant further exploration.

## MATERIALS AND METHODS

**HCT-8 intestinal epithelial cell culture.** Human ileocecal adenocarcinoma (HCT-8; ATCC CCL 244) cells were purchased from the American Type Culture Collection. Cells were maintained in T-75 (75-cm<sup>2</sup>)

tissue culture flasks as adherent monolayers in growth medium consisting of RPMI 1640 medium (catalog number 11875093) supplemented with L-glutamine and 10% heat-inactivated fetal bovine serum (FBS). Cells were stored at 37°C in a 5% CO<sub>2</sub> humidified incubator until confluence. One day prior to infection, cells were washed once with 1× phosphate-buffered saline (PBS), collected at 37°C with 0.25% trypsin-EDTA, and resuspended in growth medium. Cells were then plated (500 μL/well) into 24-well assay plates at a density of 1.14 × 10<sup>5</sup> cells/well. Cells were allowed to grow for 24 h at 37°C with 5% CO<sub>2</sub> in a humidified incubator.

***Cryptosporidium parvum* oocysts.** Oocysts of *Cryptosporidium parvum* (Iowa strain) were purchased from Waterborne, Inc., and stored at 4°C for ≤3 months in PBS with antibiotics (penicillin, streptomycin, amphotericin B, gentamicin, and 0.01% Tween 20).

**Pharmacological compounds.** Four compounds were used to modulate PKCα activity prior to *Cryptosporidium parvum* infection *in vitro*. All compounds were commercially sourced from reputable vendors and supplied as high-purity (≥95%) solids. Gö6976 and PMA were purchased from Abcam. Calphostin C was purchased from Calbiochem. Bryostatins 1 was purchased from Sigma-Aldrich. Compounds were prediluted in dimethyl sulfoxide (DMSO) at 1 mg/mL. All experiments using pharmacological compounds were performed in biological triplicate.

**C. parvum infection of HCT-8 cells.** Oocysts were excysted 24 h after seeding of HCT-8 cells, as described previously (66). Briefly, the oocysts were centrifuged at 16,000 × g for 3 min in a microcentrifuge at 4°C. Oocysts were then incubated in a 1:4 bleach solution on ice for 5 min and then centrifuged at 16,000 × g for 3 min at 4°C. The supernatant was gently aspirated, and the oocysts were resuspended in 1 mL of 1× PBS and then centrifuged for a total of three washes at 4°C. After the final wash, the supernatant was gently removed, and the oocysts were resuspended in 0.5 mL of 0.75% sodium taurocholate and incubated at 15°C for 10 min. After incubation in bile salts, the oocysts were stored in a 37°C heat block and incubated for 1 h. For heat-killed *C. parvum*, sporozoites from excysted oocysts were then incubated at 75°C for 60 s (67). After incubation, the oocysts were centrifuged at 3,000 × g for 1 min and resuspended in 0.5 mL of assay medium consisting of RPMI 1640 medium without phenol red (catalog number 11835030) supplemented with 2% heat-inactivated FBS. Oocysts were then enumerated using a disposable hemocytometer to determine the percentage of sporozoite excystation. Growth medium was gently removed from the 24-well assay plate of seeded HCT-8 cells and replaced with 0.5 mL of assay medium. Sporozoites from excysted oocysts were added to each well (5.7 × 10<sup>5</sup> sporozoites/well) of the 24-well assay plate. Plates were then spun at 150 × g for 3 min in a benchtop centrifuge at room temperature. Infected cells were incubated at 37°C with 5% CO<sub>2</sub> in a humidified incubator for 2 h.

**Stoplight immunofluorescence assay for C. parvum adherence and invasion.** After infection, assay medium containing infectious parasites was aspirated, and cells were washed with prewarmed assay medium to remove unbound parasites. Cells were then fixed with 4% paraformaldehyde for 15 min at room temperature, followed by 3 washes with 1× PBS for 3 min at room temperature. To prevent nonspecific binding, the cells were blocked with Dilution/Blocking (DB) buffer (Waterborne, Inc.) for 30 min at room temperature. Cells were stained with TRITC-conjugated Sporo-Glo (Waterborne, Inc.) diluted 1:20 in DB buffer for 1 h at room temperature protected from light. Cells were washed three times with 1× PBS supplemented with 0.01% Tween 20 (1× PBST) for 3 min. After washing, each well was permeabilized with 0.1% Triton X-100 diluted in 1× PBS for 15 min at room temperature and then washed 3 times with 1× PBST. Cells were then stained with FITC-conjugated Sporo-Glo (Waterborne, Inc.) diluted 1:20 in DB buffer for 1 h at room temperature protected from light. Cells were washed three times with 1× PBST for 3 min. To visualize HCT-8 cell nuclei, cells were stained with 4',6-diamidino-2-phenylindole (DAPI) diluted 1:1,000 in 1× PBS for 10 min at room temperature protected from light. Finally, cells were washed 3 times with 1× PBST. The cells were imaged with a Zeiss LSM 700 confocal microscope (Carl Zeiss, Inc.) using a 20× objective. Three channels were used: 405 nm for DAPI-stained nuclei, 488 nm for FITC-labeled *Cryptosporidium* parasites, and 543 nm for TRITC-labeled *Cryptosporidium* parasites.

For each assay (pharmacological inhibition/activation, dose response, and time course), 2 fields were captured for each well in biological triplicate. ZEN 2.1 Black Edition software was used to obtain z-stacks through the entire height of the cells with confocal z-slices of 1.0 μm (z-stack = 26 μm). HCT-8 cytotoxicity (number of nuclei relative to DMSO-treated controls) and contrasts in *Cryptosporidium* sporozoite adherence and invasion (cell counts relative to DMSO-treated controls) were determined. Images were processed using Fiji Is Just ImageJ (FIJI) software (version 2.0.0-rc-41/1.50d). HCT-8 cell nuclei were counted using the analyze particles command selecting for units 50 to 1,000 μm<sup>2</sup> in size. TRITC-labeled *Cryptosporidium* parasites and FITC-labeled *Cryptosporidium* parasites were counted using the analyze particles command selecting for units 2 to 20 μm<sup>2</sup> in size.

**Immunofluorescence assay for PKCα localization.** Assay medium containing infectious parasites was aspirated, and cells were washed with prewarmed assay medium to remove unbound parasites. Cells were then fixed with 4% paraformaldehyde for 15 min at room temperature. Each well was then washed three times with 1× PBS for 3 min at room temperature. After washing, each well was permeabilized with 0.1% Triton X-100 diluted in 1× PBS for 15 min at room temperature and then washed three times with 1× PBS. To prevent nonspecific binding, the cells were blocked with DB buffer for 30 min at room temperature. *C. parvum* parasites were then stained with FITC-conjugated Sporo-Glo diluted 1:20 in DB buffer for 1 h at room temperature protected from light. Cells were washed three times with 1× PBST for 3 min. HCT-8 cell PKCα was stained with an anti-PKCα antibody (catalog number ab32376; Abcam) used at a dilution of 1:200 in 1× PBS supplemented with 1% bovine serum albumin (BSA) for 1 h at room temperature. A secondary goat anti-rabbit Cy3 antibody (catalog number ab6939; Abcam) was used at a dilution of 1:1,000 in 1× PBS supplemented with 1% BSA for 1 h at room temperature

protected from light. Cells were washed three times with 1 $\times$ PBST for 3 min. HCT-8 cell nuclei were stained with DAPI diluted 1:1,000 in 1 $\times$ PBS for 10 min at room temperature protected from light. Finally, cells were washed three times with 1 $\times$  PBST and covered. The 24-well plates were imaged on a Zeiss LSM 700 confocal microscope (Carl Zeiss, Inc.) with a 63 $\times$  objective with immersion oil. Three channels were used: 405 nm for DAPI-stained nuclei, 488 nm for FITC-labeled *Cryptosporidium* parasites, and 543 nm for Cy3-labeled PKC $\alpha$ . For each well, 2 fields were captured. ZEN 2.1 Black Edition software was used to obtain z-stacks through the entire height of the cells with confocal z-slices of 1.0  $\mu$ m (z-stack = 16  $\mu$ m). HCT-8 cytotoxicity (number of nuclei relative to DMSO-treated controls) was determined. Images were processed using FIJI software.

**Cell fractionation and immunoblot analysis.** After the completion of the infection, cells were washed with prewarmed assay medium to remove unbound parasites. Each well containing *Cryptosporidium*-infected cells was treated with 0.25% trypsin-EDTA for 10 min at 37°C and collected into Eppendorf tubes. A small aliquot of cells was removed for enumeration, and the remaining cells were pelleted at 300  $\times$  *g* for 10 min. After centrifugation, cell fractionation was performed by using a commercially available cell fractionation kit (catalog number ab109719; Abcam) according to the manufacturer's instructions. Briefly, cells were resuspended in 0.1 mL of 1 $\times$  buffer A (Abcam) supplemented with a 1 $\times$  Halt protease and phosphatase inhibitor cocktail (Thermo Fisher). Cells were permeabilized with detergent I (Abcam) and then pelleted at 5,000  $\times$  *g* for 2 min and again at 10,000  $\times$  *g* for 2 min at 4°C. The resultant supernatant was collected as the cytoplasmic fraction. The cytoplasm-depleted pellet was resuspended in 0.1 mL of 1 $\times$  buffer A. The protein concentration in each fraction was quantified using a Qubit fluorometer (Thermo Fisher). Samples were prepared 1:1 with 2 $\times$  Laemmli sample buffer (Bio-Rad) and boiled for 5 min at 100°C. Samples were run on an Any kD Mini-Protean TGX polyacrylamide gel (Bio-Rad), transferred to a nitrocellulose membrane, and blocked with Intercept (PBS) blocking buffer (Li-Cor Biosciences). Anti-PKC $\alpha$  antibody was used at a dilution of 1:1,000. Secondary donkey anti-rabbit IR dye 680 (Li-Cor Biosciences) was used at a dilution of 1:10,000. Anti-GAPDH antibody (catalog number 97166; Cell Signaling Technology) was used at a dilution of 1:1,000. Secondary goat anti-mouse IR dye 800 (Li-Cor) was used at a dilution of 1:10,000. Blots were imaged with a Li-Cor Biosciences Odyssey imaging system. Images were analyzed using the analysis feature in ImageStudioLite software (version 5.2.5; Li-Cor Biosciences). The band intensity for PKC $\alpha$  under each experimental condition was measured using the analysis feature in ImageStudioLite software (version 5.2.5; Li-Cor Biosciences). PKC $\alpha$  activation (percentage of PKC $\alpha$  in the membrane fraction relative to the cytoplasmic fraction) was calculated under each condition relative to the DMSO-treated vehicle controls.

**HCT-8 cell cytotoxicity.** HCT-8 cells were assessed for the cytotoxicity of pharmacological compounds using two methods, PI staining and HCT-8 cell nucleus counts relative to DMSO-treated controls. In each case, cells were seeded (500  $\mu$ L/well) into 24-well assay plates at a density of 1.14  $\times$  10<sup>5</sup> cells/well. Cells were exposed to each experimentally matched concentration of pharmacological compounds resuspended in assay medium. Cells were incubated at 37°C with 5% CO<sub>2</sub> in a humidified incubator for 2 h. After incubation, cells were exposed to a PI-RNase A solution (Phoenix Flow Systems, Inc.). After a 30-min incubation at room temperature, the live cells were imaged on a Zeiss LSM 700 confocal microscope with a 20 $\times$  objective. The number of PI-labeled cells for exposure to each compound was calculated relative to a maximum cytotoxicity control. For further confirmation, the total number of nuclei per field for compound-exposed cells relative to DMSO-treated controls was measured.

**Data and statistical analyses.** Prism 9 (GraphPad Software, La Jolla, CA) was used for the generation of graphs and statistical analysis. Image quantification was evaluated for significance using unpaired Student's *t* test or one-way analysis of variance (ANOVA) and Tukey's *post hoc* test to determine statistical differences between means of groups of data from all tissue culture experiments. All data show the results from 1 of 2 independent experiments in biological triplicate.

## SUPPLEMENTAL MATERIAL

Supplemental material is available online only.

**SUPPLEMENTAL FILE 1**, PDF file, 0.7 MB.

## ACKNOWLEDGMENTS

This work was supported by grants from the Bill and Melinda Gates Foundation (OPP1160655 to C.M.). This research received additional funding from National Institutes of Health (NIH) grant R01AI043596 to W.A.P. and NIH grant R01AI148518 in support of C.M. S.M. was supported by University of Virginia Infectious Diseases T32 training grant TGA1007046 and an individual NIH fellowship, F30DK124003.

We thank the Advanced Microscopy Facility, which is supported by the University of Virginia School of Medicine, for training and access to the Zeiss LSM 700 scanning confocal microscope. We thank the Isakson lab at the University of Virginia for access to the Li-Cor Biosciences Odyssey imaging system.

S.M., C.M., and W.A.P. conceived and designed the experiments. S.M. performed the experiments and analyzed the data. S.M., C.M., and W.A.P. purchased the reagents and

materials. S.M. drafted the manuscript, with input from all authors. All authors have read and approved the final submission of the manuscript.

## REFERENCES

- Leitch GJ, He Q. 2012. Cryptosporidiosis—an overview. *J Biomed Res* 25: 1–16. [https://doi.org/10.1016/S1674-8301\(11\)60001-8](https://doi.org/10.1016/S1674-8301(11)60001-8).
- Ryan U, Fayer R, Xiao L. 2014. Cryptosporidium species in humans and animals: current understanding and research needs. *Parasitology* 141: 1667–1685. <https://doi.org/10.1017/S0031182014001085>.
- Steiner KL, Ahmed S, Gilchrist CA, Burkey C, Cook H, Ma JZ, Korpe PS, Ahmed E, Alam M, Kabir M, Tofail F, Ahmed T, Haque R, Petri WA, Jr, Faruque ASG. 2018. Species of cryptosporidia causing subclinical infection associated with growth faltering in rural and urban Bangladesh: a birth cohort study. *Clin Infect Dis* 67:1347–1355. <https://doi.org/10.1093/cid/ciy310>.
- Kotloff KL, Nataro JP, Blackwelder WC, Nasrin D, Farag TH, Panchalingam S, Wu Y, Sow SO, Sur D, Breiman RF, Faruque ASG, Zaidi AKM, Saha D, Alonso PL, Tamboura B, Sanogo D, Onwuchekwa U, Manna B, Ramamurthy T, Kanungo S, Ochieng JB, Omore R, Oundo JO, Hossain A, Das SK, Ahmed S, Qureshi S, Quadri F, Adegbola RA, Antonio M, Hossain MJ, Akinsola A, Mandomando I, Nhampossa T, Acácio S, Biswas K, O'Reilly CE, Mintz ED, Berkeley LY, Muhsen K, Sommerfelt H, Robins-Browne RM, Levine MM. 2013. Burden and aetiology of diarrhoeal disease in infants and young children in developing countries (the Global Enteric Multicenter Study, GEMS): a prospective, case-control study. *Lancet* 382:209–222. [https://doi.org/10.1016/S0140-6736\(13\)60844-2](https://doi.org/10.1016/S0140-6736(13)60844-2).
- Sow SO, Muhsen K, Nasrin D, Blackwelder WC, Wu Y, Farag TH, Panchalingam S, Sur D, Zaidi AKM, Faruque ASG, Saha D, Adegbola R, Alonso PL, Breiman RF, Bassat Q, Tamboura B, Sanogo D, Onwuchekwa U, Manna B, Ramamurthy T, Kanungo S, Ahmed S, Qureshi S, Quadri F, Hossain A, Das SK, Antonio M, Hossain MJ, Mandomando I, Nhampossa T, Acácio S, Omore R, Oundo JO, Ochieng JB, Mintz ED, O'Reilly CE, Berkeley LY, Livio S, Tennant SM, Sommerfelt H, Nataro JP, Ziv-Baran T, Robins-Browne RM, Mishcherkin V, Zhang J, Liu J, Houpt ER, Kotloff KL, Levine MM. 2016. The burden of cryptosporidium diarrheal disease among children < 24 months of age in moderate/high mortality regions of sub-Saharan Africa and South Asia, utilizing data from the Global Enteric Multicenter Study (GEMS). *PLoS Negl Trop Dis* 10:e0004729. <https://doi.org/10.1371/journal.pntd.0004729>.
- Mondal D, Haque R, Sack RB, Kirkpatrick BD, Petri WA, Jr. 2009. Attribution of malnutrition to cause-specific diarrheal illness: evidence from a prospective study of preschool children in Mirpur, Dhaka, Bangladesh. *Am J Trop Med Hyg* 80:824–826. <https://doi.org/10.4269/ajtmh.2009.80.824>.
- Checkley W, Epstein LD, Gilman RH, Black RE, Cabrera L, Sterling CR. 1998. Effects of Cryptosporidium parvum infection in Peruvian children: growth faltering and subsequent catch-up growth. *Am J Epidemiol* 148:497–506. <https://doi.org/10.1093/oxfordjournals.aje.a009675>.
- Guerrant DJ, Moore SR, Lima AA, Patrick PD, Schorling JB, Guerrant RL. 1999. Association of early childhood diarrhea and cryptosporidiosis with impaired physical fitness and cognitive function four-seven years later in a poor urban community in northeast Brazil. *Am J Trop Med Hyg* 61: 707–713. <https://doi.org/10.4269/ajtmh.1999.61.707>.
- Sears CL, Kirkpatrick BD. 2007. Is nitazoxanide an effective treatment for patients with acquired immune deficiency syndrome-related cryptosporidiosis? *Nat Clin Pract Gastroenterol Hepatol* 4:136–137. <https://doi.org/10.1038/ncpgasthep0737>.
- Khalil IA, Troeger C, Rao PC, Blacker BF, Brown A, Brewer TG, Colombara DV, De Hostos EL, Engmann C, Guerrant RL, Haque R, Houpt ER, Kang G, Korpe PS, Kotloff KL, Lima AAM, Petri WA, Jr, Platts-Mills JA, Shoultz DA, Forouzanfar MH, Hay SI, Reiner RC, Jr, Mokdad AH. 2018. Morbidity, mortality, and long-term consequences associated with diarrhoea from Cryptosporidium infection in children younger than 5 years: a meta-analysis study. *Lancet Glob Health* 6:e758–e768. [https://doi.org/10.1016/S2214-109X\(18\)30283-3](https://doi.org/10.1016/S2214-109X(18)30283-3).
- Forney JR, Vaughan DK, Yang S, Healey MC. 1998. Actin-dependent motility in Cryptosporidium parvum sporozoites. *J Parasitol* 84:908–913. <https://doi.org/10.2307/3284619>.
- Wetzel DM, Schmidt J, Kuhlenschmidt MS, Dubey JP, Sibley LD. 2005. Gliding motility leads to active cellular invasion by Cryptosporidium parvum sporozoites. *Infect Immun* 73:5379–5387. <https://doi.org/10.1128/IAI.73.9.5379-5387.2005>.
- Joe A, Hamer DH, Kelley MA, Pereira ME, Keusch GT, Tzipori S, Ward HD. 1994. Role of a Gal/GalNAc-specific sporozoite surface lectin in Cryptosporidium parvum-host cell interaction. *J Eukaryot Microbiol* 41:445.
- Nesterenko MV, Woods K, Upton SJ. 1999. Receptor/ligand interactions between Cryptosporidium parvum and the surface of the host cell. *Biochim Biophys Acta* 1454:165–173. [https://doi.org/10.1016/S0925-4439\(99\)00034-4](https://doi.org/10.1016/S0925-4439(99)00034-4).
- Bhat N, Joe A, Pereira Perrin M, Ward HD. 2007. Cryptosporidium p30, a galactose/N-acetylgalactosamine-specific lectin, mediates infection in vitro. *J Biol Chem* 282:34877–34887. <https://doi.org/10.1074/jbc.M706950200>.
- Forney JR, DeWald DB, Yang S, Speer CA, Healey MC. 1999. A role for host phosphoinositide 3-kinase and cytoskeletal remodeling during Cryptosporidium parvum infection. *Infect Immun* 67:844–852. <https://doi.org/10.1128/IAI.67.2.844-852.1999>.
- Elliott DA, Clark DP. 2000. Cryptosporidium parvum induces host cell actin accumulation at the host-parasite interface. *Infect Immun* 68: 2315–2322. <https://doi.org/10.1128/IAI.68.4.2315-2322.2000>.
- Guérin A, Roy NH, Kugler EM, Berry L, Burkhardt JK, Shin J-B, Striepen B. 2021. Cryptosporidium rhoptry effector protein ROP1 injected during invasion targets the host cytoskeletal modulator LMO7. *Cell Host Microbe* 29:1407–1420.e5. <https://doi.org/10.1016/j.chom.2021.07.002>.
- O'Hara SP, Chen X-M. 2011. The cell biology of Cryptosporidium infection. *Microbes Infect* 13:721–730. <https://doi.org/10.1016/j.micinf.2011.03.008>.
- Elliott DA, Coleman DJ, Lane MA, May RC, Machesky LM, Clark DP. 2001. Cryptosporidium parvum infection requires host cell actin polymerization. *Infect Immun* 69:5940–5942. <https://doi.org/10.1128/IAI.69.9.5940-5942.2001>.
- Chen X-M, O'Hara SP, Huang BQ, Splinter PL, Nelson JB, LaRusso NF. 2005. Localized glucose and water influx facilitates Cryptosporidium parvum cellular invasion by means of modulation of host-cell membrane protrusion. *Proc Natl Acad Sci U S A* 102:6338–6343. <https://doi.org/10.1073/pnas.0408563102>.
- Delling C, Dausgschies A, Bangoura B, Dengler F. 2019. Cryptosporidium parvum alters glucose transport mechanisms in infected enterocytes. *Parasitol Res* 118:3429–3441. <https://doi.org/10.1007/s00436-019-06471-y>.
- Yang Y-L, Buck GA, Widmer G. 2010. Cell sorting-assisted microarray profiling of host cell response to Cryptosporidium parvum infection. *Infect Immun* 78:1040–1048. <https://doi.org/10.1128/IAI.01009-09>.
- Mauzy MJ, Enomoto S, Lancto CA, Abrahamson MS, Rutherford MS. 2012. The Cryptosporidium parvum transcriptome during in vitro development. *PLoS One* 7:e31715. <https://doi.org/10.1371/journal.pone.0031715>.
- Tandel J, English ED, Sateriale A, Gullicksrud JA, Beiting DP, Sullivan MC, Pinkston B, Striepen B. 2019. Life cycle progression and sexual development of the apicomplexan parasite Cryptosporidium parvum. *Nat Microbiol* 4:2226–2236. <https://doi.org/10.1038/s41564-019-0539-x>.
- Upton SJ, Tilley M, Brillhart DB. 1994. Comparative development of Cryptosporidium parvum (Apicomplexa) in 11 continuous host cell lines. *FEMS Microbiol Lett* 118:233–236. <https://doi.org/10.1111/j.1574-6968.1994.tb06833.x>.
- Hashim A, Mulcahy G, Bourke B, Clyne M. 2006. Interaction of Cryptosporidium hominis and Cryptosporidium parvum with primary human and bovine intestinal cells. *Infect Immun* 74:99–107. <https://doi.org/10.1128/IAI.74.1.99-107.2006>.
- Castellanos-Gonzalez A, Sparks H, Nava S, Huang W, Zhang Z, Rivas K, Hulverson MA, Barrett LK, Ojo KK, Fan E, Van Voorhis WC, White AC. 2016. A novel calcium-dependent kinase inhibitor, bumped kinase inhibitor 1517, cures cryptosporidiosis in immunosuppressed mice. *J Infect Dis* 214:1850–1855. <https://doi.org/10.1093/infdis/jiw481>.
- Wojcik GL, Korpe P, Marie C, Mentzer AJ, Carstensen T, Mychaleckyj J, Kirkpatrick BD, Rich SS, Concannon P, Faruque ASG, Haque R, Petri WA, Jr, Duggal P. 2020. Genome-wide association study of cryptosporidiosis in infants implicates PRKCA. *mBio* 11:e03343-19. <https://doi.org/10.1128/mBio.03343-19>.
- Love MS, Beasley FC, Jumani RS, Wright TM, Chatterjee AK, Huston CD, Schultz PG, McNamara CW. 2017. A high-throughput phenotypic screen identifies clofazimine as a potential treatment for cryptosporidiosis. *PLoS Negl Trop Dis* 11:e0005373. <https://doi.org/10.1371/journal.pntd.0005373>.

31. Martiny-Baron G, Kazanietz MG, Mischak H, Blumberg PM, Kochs G, Hug H, Marmé D, Schächtele C. 1993. Selective inhibition of protein kinase C isozymes by the indolocarbazole Gö 6976. *J Biol Chem* 268:9194–9197. [https://doi.org/10.1016/S0021-9258\(18\)98335-3](https://doi.org/10.1016/S0021-9258(18)98335-3).
32. Liu T-L, Fan X-C, Li Y-H, Yuan Y-J, Yin Y-L, Wang X-T, Zhang L-X, Zhao G-H. 2018. Expression profiles of mRNA and lncRNA in HCT-8 cells infected with *Cryptosporidium parvum* Ild subtype. *Front Microbiol* 9:1409. <https://doi.org/10.3389/fmicb.2018.01409>.
33. Black A, Black J. 2013. Protein kinase C signaling and cell cycle regulation. *Front Immunol* 3:423. <https://doi.org/10.3389/fimmu.2012.00423>.
34. Pontremoli S, Melloni E, Michetti M, Salamino F, Sparatore B, Sacco O, Horecker BL. 1986. Differential mechanisms of translocation of protein kinase C to plasma membranes in activated human neutrophils. *Biochem Biophys Res Commun* 136:228–234. [https://doi.org/10.1016/0006-291x\(86\)90898-3](https://doi.org/10.1016/0006-291x(86)90898-3).
35. Strulovici B, Daniel-Issakani S, Oto E, Nestor J, Chan H, Tsou AP. 1989. Activation of distinct protein kinase C isozymes by phorbol esters: correlation with induction of interleukin 1 beta gene expression. *Biochemistry* 28:3569–3576. <https://doi.org/10.1021/bi00434a063>.
36. Abdullah LH, Conway JD, Cohn JA, Davis CW. 1997. Protein kinase C and Ca<sup>2+</sup> activation of mucin secretion in airway goblet cells. *Am J Physiol* 273:L201–L210. <https://doi.org/10.1152/ajplung.1997.273.1.L201>.
37. Karanis P, Aldeyari HM. 2011. Evolution of *Cryptosporidium* in vitro culture. *Int J Parasitol* 41:1231–1242. <https://doi.org/10.1016/j.ijpara.2011.08.001>.
38. Mele R, Gomez Morales MA, Tosini F, Pozio E. 2004. *Cryptosporidium parvum* at different developmental stages modulates host cell apoptosis in vitro. *Infect Immun* 72:6061–6067. <https://doi.org/10.1128/IAI.72.10.6061-6067.2004>.
39. Borowski H, Thompson RCA, Armstrong T, Clode PL. 2010. Morphological characterization of *Cryptosporidium parvum* life-cycle stages in an in vitro model system. *Parasitology* 137:13–26. <https://doi.org/10.1017/S003182009990837>.
40. Jalava A, Lintunen M, Heikkilä J. 1993. Protein kinase C- $\alpha$  but not protein kinase C- $\epsilon$  is differentially down-regulated by bryostatin 1 and tetradecanoyl phorbol 13-acetate in SH-SY5Y human neuroblastoma cells. *Biochem Biophys Res Commun* 191:472–478. <https://doi.org/10.1006/bbrc.1993.1242>.
41. Lee H-W, Smith L, Pettit GR, Vinitzky A, Smith JB. 1996. Ubiquitination of protein kinase C- $\alpha$  and degradation by the proteasome. *J Biol Chem* 271:20973–20976. <https://doi.org/10.1074/jbc.271.35.20973>.
42. Szallasi Z, Denning MF, Smith CB, Dlugosz AA, Yuspa SH, Pettit GR, Blumberg PM. 1994. Bryostatin 1 protects protein kinase C-delta from down-regulation in mouse keratinocytes in parallel with its inhibition of phorbol ester-induced differentiation. *Mol Pharmacol* 46:840–850.
43. Lorenzo PS, Bögi K, Hughes KM, Beheshti M, Bhattacharyya D, Garfield SH, Pettit GR, Blumberg PM. 1999. Differential roles of the tandem C1 domains of protein kinase C  $\delta$  in the biphasic down-regulation induced by bryostatin 1. *Cancer Res* 59:6137–6144.
44. Bruns RF, Miller FD, Merriman RL, Howbert JJ, Heath WF, Kobayashi E, Takahashi I, Tamaoki T, Nakano H. 1991. Inhibition of protein kinase C by calphostin C is light-dependent. *Biochem Biophys Res Commun* 176:288–293. [https://doi.org/10.1016/0006-291x\(91\)90922-t](https://doi.org/10.1016/0006-291x(91)90922-t).
45. Redman C, Lefevre J, MacDonald ML. 1995. Inhibition of diacylglycerol kinase by the antitumor agent calphostin C. Evidence for similarity between the active site of diacylglycerol kinase and the regulatory site of protein kinase C. *Biochem Pharmacol* 50:235–241. [https://doi.org/10.1016/0006-2952\(95\)00118-j](https://doi.org/10.1016/0006-2952(95)00118-j).
46. Hryciw DH, Pollock CA, Poronnik P. 2005. PKC- $\alpha$ -mediated remodeling of the actin cytoskeleton is involved in constitutive albumin uptake by proximal tubule cells. *Am J Physiol Renal Physiol* 288:F1227–F1235. <https://doi.org/10.1152/ajprenal.00428.2003>.
47. Peng J, He F, Zhang C, Deng X, Yin F. 2011. Protein kinase C- $\alpha$  signals P115RhoGEF phosphorylation and RhoA activation in TNF- $\alpha$ -induced mouse brain microvascular endothelial cell barrier dysfunction. *J Neuroinflammation* 8:28. <https://doi.org/10.1186/1742-2094-8-28>.
48. Chen X-M, Huang BQ, Splinter PL, Cao H, Zhu G, McNiven MA, LaRusso NF. 2003. *Cryptosporidium parvum* invasion of biliary epithelia requires host cell tyrosine phosphorylation of cortactin via c-Src. *Gastroenterology* 125:216–228. [https://doi.org/10.1016/s0016-5085\(03\)00662-0](https://doi.org/10.1016/s0016-5085(03)00662-0).
49. Chen X-M, O'Hara SP, Huang BQ, Nelson JB, Lin JJ-C, Zhu G, Ward HD, LaRusso NF. 2004. Apical organelle discharge by *Cryptosporidium parvum* is temperature, cytoskeleton, and intracellular calcium dependent and required for host cell invasion. *Infect Immun* 72:6806–6816. <https://doi.org/10.1128/IAI.72.12.6806-6816.2004>.
50. Chen X-M, Splinter PL, Tietz PS, Huang BQ, Billadeau DD, LaRusso NF. 2004. Phosphatidylinositol 3-kinase and frabin mediate *Cryptosporidium parvum* cellular invasion via activation of Cdc42. *J Biol Chem* 279:31671–31678. <https://doi.org/10.1074/jbc.M401592200>.
51. Brandt D, Gimona M, Hillmann M, Haller H, Mischak H. 2002. Protein kinase C induces actin reorganization via a Src- and Rho-dependent pathway. *J Biol Chem* 277:20903–20910. <https://doi.org/10.1074/jbc.M200946200>.
52. Li D, Shatos MA, Hodges RR, Dartt DA. 2013. Role of PKC $\alpha$  activation of Src, PI-3K/AKT, and ERK in EGF-stimulated proliferation of rat and human conjunctival goblet cells. *Invest Ophthalmol Vis Sci* 54:5661–5674. <https://doi.org/10.1167/iovs.13-12473>.
53. Ziemba BP, Burke JE, Masson G, Williams RL, Falke JJ. 2016. Regulation of PI3K by PKC and MARCKS: single-molecule analysis of a reconstituted signaling pathway. *Biophys J* 110:1811–1825. <https://doi.org/10.1016/j.bpj.2016.03.001>.
54. Hsu AH, Lum MA, Shim K-S, Frederick PJ, Morrison CD, Chen B, Lele SM, Sheinin YM, Daikoku T, Dey SK, Leone G, Black AR, Black JD. 2018. Crosstalk between PKC $\alpha$  and PI3K/AKT signaling is tumor suppressive in the endometrium. *Cell Rep* 24:655–669. <https://doi.org/10.1016/j.celrep.2018.06.067>.
55. Chen L, Hahn H, Wu G, Chen CH, Liron T, Schechtman D, Cavallaro G, Banci L, Guo Y, Bolli R, Dorn GW, Mochly-Rosen D. 2001. Opposing cardioprotective actions and parallel hypertrophic effects of delta PKC and epsilon PKC. *Proc Natl Acad Sci U S A* 98:11114–11119. <https://doi.org/10.1073/pnas.191369098>.
56. Song JC, Rangachari PK, Matthews JB. 2002. Opposing effects of PKC $\alpha$  and PKC $\epsilon$  on basolateral membrane dynamics in intestinal epithelia. *Am J Physiol Cell Physiol* 283:C1548–C1556. <https://doi.org/10.1152/ajpcell.00105.2002>.
57. Braun MU, Mochly-Rosen D. 2003. Opposing effects of  $\delta$ - and  $\zeta$ -protein kinase C isozymes on cardiac fibroblast proliferation: use of isozyme-selective inhibitors. *J Mol Cell Cardiol* 35:895–903. [https://doi.org/10.1016/S0022-2828\(03\)00142-1](https://doi.org/10.1016/S0022-2828(03)00142-1).
58. Liu J, Van Blitterswijk CA, De Boer J. 2008. Different protein kinase C isozymes exert opposing effects on osteogenesis of human mesenchymal stem cells, p 1563. *In Proceedings of the 8th World Biomaterials Congress 2008*. Curran Associates, Red Hook, NY.
59. Neurotrope Bioscience, Inc. 2018. A randomized, double-blind, placebo-controlled, phase 2 study assessing the safety, tolerability and efficacy of bryostatin in the treatment of moderately severe to severe Alzheimer's disease. *ClinicalTrials.gov* identifier NCT02431468.
60. Rawal S, Majumdar S, Vohra H. 2005. Activation of MAPK kinase pathway by Gal/GalNAc adherence lectin of *E. histolytica*: gateway to host response. *Mol Cell Biochem* 268:93–101. <https://doi.org/10.1007/s11010-005-3698-4>.
61. GTEx Consortium. 2015. The Genotype-Tissue Expression (GTEx) pilot analysis: multitissue gene regulation in humans. *Science* 348:648–660. <https://doi.org/10.1126/science.1262110>.
62. Baltuch GH, Dooley NP, Rostworowski KM, Villemure JG, Yong VW. 1995. Protein kinase C isoform alpha overexpression in C6 glioma cells and its role in cell proliferation. *J Neurooncol* 24:241–250. <https://doi.org/10.1007/BF01052840>.
63. Zhao GH, Fang YQ, Ryan U, Guo YX, Wu F, Du SZ, Chen DK, Lin Q. 2016. Dynamics of Th17 associating cytokines in *Cryptosporidium parvum*-infected mice. *Parasitol Res* 115:879–887. <https://doi.org/10.1007/s00436-015-4831-2>.
64. Meisel M, Hermann-Kleiter N, Hinterleitner R, Gruber T, Wachowicz K, Pfeifferhofer-Obermair C, Fresser F, Leitges M, Soldani C, Viola A, Kaminski S, Baier G. 2013. The kinase PKC $\alpha$  selectively upregulates interleukin-17A during Th17 cell immune responses. *Immunity* 38:41–52. <https://doi.org/10.1016/j.immuni.2012.09.021>.
65. Solaymani-Mohammadi S, Singer SM. 2013. Regulation of intestinal epithelial cell cytoskeletal remodeling by cellular immunity following gut infection. *Mucosal Immunol* 6:369–378. <https://doi.org/10.1038/mi.2012.80>.
66. Pawlowic MC, Vinayak S, Sateriale A, Brooks CF, Striepen B. 2017. Generating and maintaining transgenic *Cryptosporidium parvum* parasites. *Curr Protoc Microbiol* 46:20B.2.1–20B.2.32. <https://doi.org/10.1002/cpmc.33>.
67. Moriarty EM, Duffy G, McEvoy JM, Caccio S, Sheridan JJ, McDowell D, Blair IS. 2005. The effect of thermal treatments on the viability and infectivity of *Cryptosporidium parvum* on beef surfaces. *J Appl Microbiol* 98:618–623. <https://doi.org/10.1111/j.1365-2672.2004.02498.x>.